Photoselective excited state dynamics in ZnO–Au nanocomposites and their implications in photocatalysis and dye-sensitized solar cells†

Soumik Sarkar,[a] Abhinandan Makhal,[a] Tanujjal Bora,[b] Sunandan Baruah,[b] Joydeep Dutta[b] and Samir Kumar Pal‡*[a]

Improving the performance of photoactive solid-state devices begins with systematic studies of the metal–semiconductor nanocomposites (NCs) upon which such devices are based. Here, we report the photo-dependent excitonic mechanism and the charge migration kinetics in a colloidal ZnO–Au NC system. By using a picosecond-resolved Förster resonance energy transfer (FRET) technique, we have demonstrated that excited ZnO nanoparticles (NPs) resonantly transfer visible optical radiation to the Au NPs, and the quenching of defect-mediated visible emission depends solely on the excitation level of the semiconductor. The role of the gold layer in promoting photolytic charge transfer, the activity of which is dependent upon the degree of excitation, was probed using methylene blue (MB) reduction at the semiconductor interface. Incident photon-to-current efficiency measurements show improved charge injection from a sensitizing dye to a semiconductor electrode in the presence of gold in the visible region. Furthermore, the short-circuit current density and the energy conversion efficiency of the ZnO–Au NP based dye-sensitized solar cell (DSSC) are much higher than those of a DSSC comprised of only ZnO NP. Our results represent a new paradigm for understanding the mechanism of defect-state passivation and photolytic activity of the metal component in metal–semiconductor nanocomposite systems.

1. Introduction

Quantum dots and metal nanoparticles (NPs) are of great interest because of their unique electronic, optical, and magnetic properties.[1–5] In particular, noble metal NPs having diameters below 10 nm have been the focus of recent works[6,7] due in part to their enhanced reactivities. For example, Au NPs of 3 to 8 nm diameter have been shown to tune the catalytic properties of TiO_2.[8–10] In the structure of composite nanocluster-based dye-sensitized solar cells (DSSCs), Au NPs are employed to facilitate efficient charge separation, thus serving as a Schottky barrier for reducing the rate of electron–hole recombination.[11] Yang and Tetsu [12] studied the enhancement of anodic photocurrents induced by visible light irradiation in a device based on Au NPs deposited on TiO_2 films. Their data indicate that using Au Schottky contacts in photovoltaic cells may yield improved device performance. In an earlier investigation[13] by Kamat and co-workers, it was shown that the photoelectro-chemical performance of nanostructured TiO_2 films could be improved by coupling to noble metal NPs. Using the hypothesis of Fermi level equilibration, it has been possible to understand the increase in the photo-voltage of TiO_2–Au films[13,14] as well as the charging effects in metal–semiconductor colloids.[15–18] Although there have been many attempts to obtain improved device performance with metal–semiconductor nanocomposites (NCs), the mechanism of charge separation as well as the excitation-dependent interfacial charge transfer kinetics in the nanoscale regime are yet to be fully understood.

The improved performance of photoactive processes and devices has typically been achieved with composite nanostructures based on semiconductor oxides, such as TiO_2 and ZnO, modified with noble metal NPs. A systematic study of the energetics of such NC systems is important for tailoring the properties of next-generation nano-devices. The mediating role of noble metals in storing and shuttling photogenerated electrons from the semiconductor to an acceptor in a photocatalytic process can be understood by designing metal–semiconductor NC structures. Among direct band-gap crystals, ZnO has a wide band gap of 3.37 eV and a large

[a] Department of Chemical, Biological and Macromolecular Sciences, Unit for Nano Science & Technology, S. N. Bose National Centre for Basic Sciences, Block JD, Sector III, Salt Lake, Kolkata 700 098, India. E-mail: skpal@bose.res.in
[b] Centre of Excellence in Nanotechnology, School of Engineering and Technology, Asian Institute of Technology, Klong Luang, Pathumthani 12120, Thailand

† Electronic supplementary information (ESI) available: TEM images, particle size distribution of both ZnO NPs and ZnO–Au NCs. Picosecond-resolved study of ZnO–Au NC upon excitation above the band-edge. See DOI: 10.1039/c1cp20892f
‡ Present address: Arthur Amos Noyes Laboratory of Chemical Physics California Institute of Technology (CALTECH), 1200 East California Boulevard, Pasadena, CA 91125, USA. E-mail: spal@caltech.edu

12488 | *Phys. Chem. Chem. Phys.*, 2011, **13**, 12488–12496

This journal is © the Owner Societies 2011

exciton binding energy of 60 meV at room temperature. Two photoluminescence (PL) bands are usually found: a relatively weak and narrow UV emission band (band-gap emission) around 370 nm (3.35 eV), which is just below the onset of absorption, and a much stronger and broader visible emission band with a maximum near 550 nm (2.25 eV). The UV emission band is due to the radiative annihilation of excitons, the high binding energy of which permits observation even at significantly elevated temperatures.[19] The green emission is known to come from the defect centers located near the surface of the NPs.[20] Numerous studies have been conducted to improve the band-gap emission by controlling the influence of defect states for the improvement of emission efficiency in semiconductors.[21,22] In an earlier study[23] with ZnO–Pt NCs, it was reported that the band-gap emission is enhanced substantially, while the defect emission is suppressed. The underlying mechanism behind enhancement of the band-gap emission and quenching of the defect-mediated green emission is a combination of the energy transfer between defects and surface plasmon (SP) resonance in Pt NPs, as well as electron–hole pair generation and recombination processes in ZnO nanorods. A similar study[24] with Au-capped ZnO nanorods also indicates that the suppression of the green emission might be due to a combined effect of Au SP and passivation of the ZnO nanorod surface traps.

The present study is aimed at elucidating the mechanism of pronounced intrinsic emission from colloidal ZnO and ZnO–Au NCs upon above band-edge and below band-gap excitation. To probe the correlation between dynamics of photo-generated carrier trapping at the defect sites and kinetics of charge migration from ZnO and ZnO–Au semiconductors, methylene blue (MB) degradation was examined using UV light and optical filters. Photostability and luminescence studies from a ZnO–Au NC colloidal dispersion show that Förster resonance energy transfer (FRET) dynamics from a donor semiconductor to gold acceptor can be observed. Finally, we have designed a model DSSC based on ZnO NPs which leads to an increase in short-circuit photo-current (J_{sc}) and improved overall efficiency (η) in the presence of Au NPs. The reason behind the giant improvement in efficiency is also clarified by photoconductivity measurements of the ZnO NP and ZnO–Au NC thin films.

2. Experimental

2.1 Preparation of ZnO and ZnO–Au nanocolloids

In order to synthesize colloidal solution of ZnO NPs, zinc acetate dihydrate, $Zn(CH_3COO)_2 \cdot 2H_2O$ (Merck), was used as starting material. 20 ml of 4 mM zinc acetate solution was prepared in ethanol (Merck) followed by a dilution up to 50% by adding another 20 ml of fresh ethanol to the solution. Then 20 ml of 4 mM NaOH solution in ethanol was added to it under constant stirring. The reaction beaker was then kept in a preheated water bath at 60 °C for 2 h to hydrolyse, after which a transparent ZnO NP colloid was obtained.

ZnO–Au NC colloid was prepared by in situ synthesis of Au NPs on the surface of the ZnO NPs. 5 ml of 1 mM chloroauric acid [$HAuCl_4 \cdot H_2O$] (Sigma) ethanolic solution was slowly added to the as synthesized ZnO NP colloid under constant stirring at room temperature. The stirring was continued for 15 min. Then 7 ml of 5 mM sodium borohydride, $NaBH_4$ (Sigma), in ethanol solution was added drop-wise to the solution in order to reduce the gold chloride to Au NPs. Immediately after adding $NaBH_4$ the solution becomes red from pale yellow color indicating the formation of the Au NPs in the ZnO NP colloid. The weight ratio between ZnO and Au after the preparation process was found to be 1.3 : 1 (see ESI†). The colloidal solutions of ZnO NPs and ZnO–Au NCs are used to perform all the spectroscopic studies.

2.2 Dye sensitization and solar cell construction

500 nm thick films of ZnO NPs and ZnO–Au NCs were prepared by dropping 100 μl of the respective colloid on a FTO glass substrate (Asahi Japan). The drop was uniformly spread over the substrate and allowed to dry at 60 °C. The process was repeated several times in order to achieve the desired thickness of the film, following which the photoelectrodes were annealed at 350 °C for 2 h in atmospheric conditions. Dye adsorption was carried out by dipping the photoelectrodes into a 0.5 mM dye N719 (Solaronix, Switzerland) in ethanol solution for 24 h in dark at room temperature. After 24 h, the substrates were withdrawn from the dye solution and rinsed with ethanol several times in order to remove the excess dye on the film surface. The photoelectrodes were then allowed to dry in dark at room temperature in a controlled humidity chamber (40% humidity) for 2 h.

FTO glass with a thin platinum layer, deposited on the FTO surface by thermal decomposition of platinum chloride, [$H_2PtCl_6 \cdot H_2O$] (Fluka) at 385 °C for 15 min, was used as a counter electrode. Counter electrodes were placed on top of the photoelectrodes to form the photovoltaic cells. A single layer of 50 μm thick surlyn 1702 (Dupont) was used as a spacer between the two electrodes and the cells were sealed by applying heat and pressure simultaneously. Finally the liquid electrolyte consisting of 0.5 M lithium iodide (LiI), 0.05 M iodine (I_2) and 0.5 M 4-tert-butylpyridine (TBP) in acetonitrile (ACN) was filled in the cells through the two small holes (diameter = 1 mm) pre-drilled on the counter electrodes. The two holes were finally sealed by surlyn to prevent any electrolyte leakage from the cells. Photocurrent measurements of the DSSC were performed under a High Power Xenon (Europe/USA) light source (power consumption = 90 W, light intensity = 10.5 klux).

2.3 Microscopy and optical measurements

Transmission electron microscopy (TEM) was carried out by applying a drop of the ZnO and ZnO–Au samples to carbon-coated copper grids. Particle sizes were determined from micrographs recorded at a magnification of 100000× using an FEI (Technai S-Twin, operating at 200 kV) instrument at SINP, India. Steady-state absorption and emission spectra were measured with a Shimadzu UV-2450 spectrophotometer and a Jobin Yvon Fluoromax-3 fluorimeter (pump power at 320 nm is ∼22 μW cm^{-2}), respectively. All the photoluminescence transients were measured using the picosecond-resolved time-correlated single photon counting (TCSPC) technique,

This journal is © the Owner Societies 2011

Phys. Chem. Chem. Phys., 2011, **13**, 12488–12496 | 12489

a commercially available picosecond diode laser-pumped (LifeSpec-ps) time-resolved fluorescence spectrophotometer from Edinburgh Instruments, UK. Picosecond excitation pulses from the picoquant diode laser were used at 375 nm with an instrument response function (IRF) of 60 ps. A micro channel-plate-photomultiplier tube (MCP-PMT, Hammamatsu) was used to detect the photoluminescence from the sample after dispersion through a monochromator. For all transients the polarizer on the emission side was adjusted to be at 55° (Magic angle) with respect to the polarization axis of the excitation beam.

2.4 Data analysis

Curve fitting of observed fluorescence transients was carried out using a nonlinear least square fitting procedure to a function $\left(X(t) = \int_0^t E(t')R(t-t')dt'\right)$ comprised of convolution of the IRF $(E(t))$ with a sum of exponentials $\left(R(t) = A + \sum_{i=1}^N B_i e^{-t/\tau_i}\right)$ with pre-exponential factors (B_i), characteristic lifetimes (τ_i) and a background (A). The relative concentration in a multiexponential decay is expressed as $c_n = \frac{B_n}{\sum_{i=1}^N B_i} \times 100$. The average lifetime (amplitude-weighted) of a multiexponential decay[25] is expressed as, $\tau_{av} = \sum_{i=1}^N c_i \tau_i$.

3. Results and discussion

3.1 Spectroscopic studies

The structure, crystalline phase, size, and morphology of ZnO NPs and ZnO–Au NCs were determined (with TEM). Representative high-resolution TEM (HRTEM) images of the ZnO–Au NCs are illustrated in Fig. 1a, where the measured average diameter is 6 and 8 nm for ZnO and Au NPs, respectively. From TEM observation it was found that the ZnO–Au NCs are fairly monodisperse and their shapes are different from that of the spherical ZnO NPs due to the incorporation of Au components. The higher contrast of Au observed in the TEM image is due to the higher electron density of metallic Au compared to semiconducting ZnO. The relevant TEM images are shown in ESI† (Fig. S1–S3).

The visible absorption spectrum of gold grown onto the ZnO NPs was clearly characterized by the plasmon resonance peak of Au NPs. Fig. 1b shows the absorption spectra of the ZnO–Au NCs and pure ZnO NPs. It is generally believed that the band-edge absorption of a semiconductor in the quantum-confined size regime (≤ 7 nm) is dependent on the particle size.[26] There is no distinct variation in absorption characteristics in the range 300 to 420 nm, which implies that no apparent growth of ZnO NPs occurred during the formation of Au on ZnO NPs. An SP band, resulting from Au in the ZnO–Au NCs, centered at ~ 525 nm can also be observed in the NC (Fig. 1b). In Fig. 2a we have plotted the excitation spectra of bare ZnO NPs and ZnO–Au NCs monitored at the emission peaks (368 nm and 550 nm, respectively). The room temperature PL spectra of both the bare ZnO NPs and ZnO–Au NCs (Fig. 2b) are comprised of one broad emission band upon excitation below the band-gap ($\lambda_{ex} = 375$ nm) and two emission bands upon excitation above the band-edge
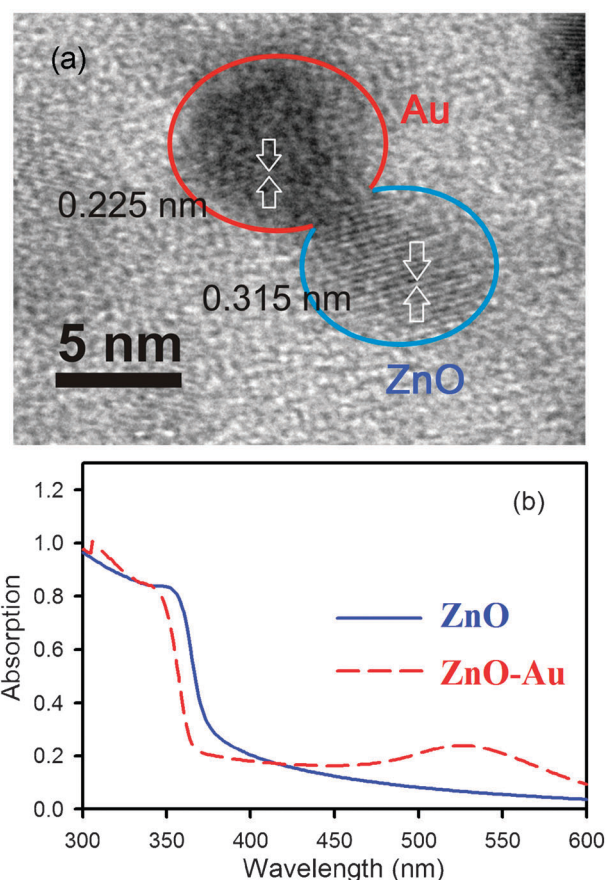

Fig. 1 (a) High-resolution TEM (HRTEM) image of dumbbell-like ZnO–Au NCs with Au attached to the ZnO surface. (b) Steady state absorption spectra of bare ZnO NPs (blue) and ZnO–Au NCs (red) showing the SP band at 520 nm.

($\lambda_{ex} = 320$ nm). The narrow UV band centered at 368 nm is due to exciton recombination. The broad visible emission arises from the defect centers located near the surface. van Dijken et al.[27] proposed that the visible band emission is due to recombination of an electron from the conduction band with a deep electron trapping center of doubly charged oxygen vacancies (V_O^{++}). Vanheusden et al.[28] however suggested that the recombination of isolated singly charged V_O^+ centers with photoexcited holes is responsible for the green emission characteristics of ZnO materials. Analysis of the broad emission observed in our sample in the blue-green region shows that it is composed of two emission bands (shown as dotted lines in Fig. 2b (inset)) which are marked as P1 and P2.[29] The characteristics of each emission band depend upon whether it arises from a doubly charged vacancy center V_O^{++} (P2) or a singly charged vacancy center V_O^+ (P1). The V_O^{++} center, created by capture of a hole by the V_O^+ center in a depletion region, leads to the P2 emission line. The singly charged center (V_O^+) in the absence of a depletion region turns into a neutral center ($V_O^\times$) upon the capture of an electron (n-type ZnO) from the conduction band which then recombines with a hole in the valence band giving rise to the P1 emission.[30] The spectral content of the blue-green band is determined by the relative weight of the two overlapping emission peaks.

As shown in Fig. 2b, when excitation below the band-gap ($\lambda_{ex} = 375$ nm) was used, the defect-related emission is
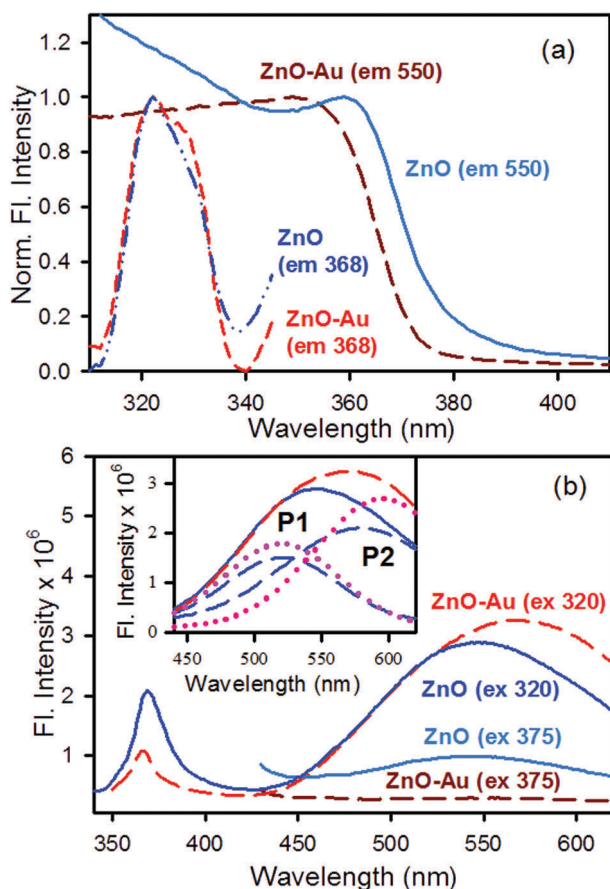
12490 | *Phys. Chem. Chem. Phys.*, 2011, **13**, 12488–12496

This journal is © the Owner Societies 2011

Fig. 2 (a) Excitation spectra of ZnO NPs (blue) and ZnO–Au NCs (red) monitored at 368 nm and 550 nm. (b) Steady state emission spectra of ZnO NPs (blue) and ZnO–Au NCs (red) are shown (excitation at 320 and 375 nm). The inset shows that the defect related green emission is composed of two bands, P1 and P2 (see text).

suppressed in the presence of Au NPs. Herein, we propose FRET from a donor ZnO NP to Au acceptor, which is responsible for the observed suppression of emission bands. The mechanism of FRET involves a donor in an excited electronic state, which may transfer its excitation energy to a nearby acceptor in a nonradiative fashion through long range dipole–dipole interaction.[25] The theory is based on the concept of treating an excited donor as an oscillating dipole that can undergo energy exchange with a second dipole having a similar resonance frequency. In principle, if the fluorescence emission spectrum of the donor molecule overlaps the absorption spectrum of an acceptor molecule, and the two are within a minimal distance from one another (1–10 nm), the donor can directly transfer its excitation energy to the acceptor *via* exchange of a virtual photon. The spectral overlap of the ZnO emission spectrum with that of the Au absorption spectrum is shown in Fig. 3a. The faster excited state lifetime of the ZnO–Au NC with respect to that of the free ZnO NP is clearly noticeable from Fig. 3b. Details of the spectroscopic parameters and the fitting parameters of the fluorescence decays are tabulated in Table 1. In order to estimate FRET efficiency of the donor (ZnO) and hence to determine distances of donor–acceptor pairs, we followed the methodology
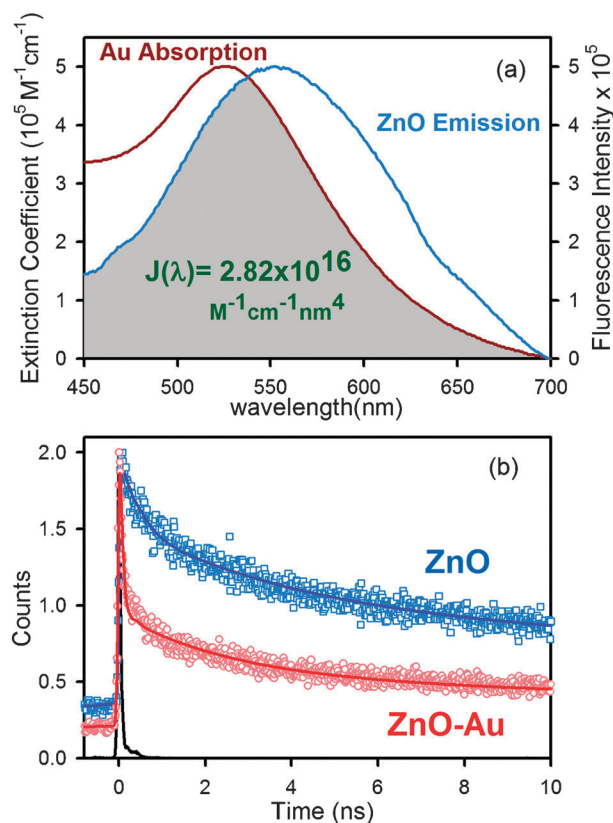

Fig. 3 (a) SP band of Au NPs and emission spectra of ZnO NPs are shown. An overlapping zone between emission of ZnO NPs and absorption of acceptor Au is indicated as a gray shaded zone. (b) The picosecond-resolved fluorescence transients of ZnO NPs, in the absence (blue) and presence of acceptor Au (red) (excitation at 375 nm), collected at 550 nm.

described in chapter 13 of ref. 25. The Förster distance (R_0) is given by,

$$R_0 = 0.211 \times [\kappa^2 n^{-4} Q_D J(\lambda)]^{\frac{1}{6}} \ (\text{in Å}) \qquad (1)$$

where, κ^2 is a factor describing the relative orientation in space of the transition dipoles of the donor and acceptor. For donors and acceptors that randomize by rotational diffusion prior to energy transfer, the magnitude of κ^2 is assumed to be $2/3$.[25,31] The refractive index (n) of the medium is 1.4, and the quantum yield (Q_D) of the donor in the absence of an acceptor is measured to be 3.8×10^{-3}. $J(\lambda)$, the overlap integral, which expresses the degree of spectral overlap between the donor emission and the acceptor absorption is given by,

$$J(\lambda) = \frac{\int_0^\infty F_D(\lambda)\varepsilon_A(\lambda)\lambda^4 \mathrm{d}\lambda}{\int_0^\infty F_D(\lambda)\mathrm{d}\lambda} \qquad (2)$$

where $F_D(\lambda)$ is the fluorescence intensity of the donor in the wavelength range of λ to $\lambda + \mathrm{d}\lambda$ and is dimensionless. $\varepsilon_A(\lambda)$ is the extinction coefficient (in $M^{-1} cm^{-1}$) of the acceptor at λ. If λ is in nm, then $J(\lambda)$ is in units of $M^{-1} cm^{-1} nm^4$. The estimated value of the overlap integral is 2.82×10^{16}.

This journal is © the Owner Societies 2011

Phys. Chem. Chem. Phys., 2011, **13**, 12488–12496 | 12491

Table 1 Dynamics of picosecond-resolved luminescence transients of ZnO NPs in the presence and absence of Au NPs[a] and the kinetics parameters[b] for the photoselective degradation of Methylene Blue in the presence of ZnO and ZnO–Au nanocolloids

Dynamics study

Samples	τ_1	τ_2	τ_3	τ_{avg}
ZnO NP (bare)	47.58 ns (41%)	3.78 ns (23%)	0.280 ns (36%)	20.48 ns
ZnO–Au NC	33.34 ns (8%)	2.60 ns (10%)	0.051 ns (82%)	2.97 ns

Kinetics study [$y = A\exp(-kt) + y_0$]

Samples and filters	K (s^{-1})	A (%)	R^2
ZnO (420 HP)	1.055×10^{-3}	2.66	0.9644
ZnO–Au (420 HP)	1.388×10^{-3}	2.78	0.9378
ZnO (460 LP)	2.203×10^{-3}	11.68	0.9704
ZnO–Au (460 LP)	2.528×10^{-3}	29.31	0.9961
ZnO (320 HP–460 LP)	2.340×10^{-3}	23.55	0.9939
ZnO–Au (320 HP–460 LP)	2.287×10^{-3}	19.65	0.9985

[a] The emissions from ZnO NPs and ZnO–Au NCs (probing at 550 nm) were detected with a 375 nm laser excitation. Numbers in the parentheses indicate relative weightage. [b] Kinetic constants (k), regression coefficients (R^2) and the percentages of photoselective degradation (A). The optical filters used in the study are indicated in parentheses.

Once the value of R_0 is known, the donor–acceptor distance (r) can be easily calculated using the formula,

$$r^6 = \frac{[R_0^6(1 - E)]}{E} \quad (3)$$

Here E is the efficiency of energy transfer. The transfer efficiency is measured using the relative fluorescence lifetime of the donor, in the absence (τ_D) and presence (τ_{DA}) of the acceptor.

$$E = 1 - \frac{\tau_{DA}}{\tau_D} \quad (4)$$

From the average lifetime calculation for the ZnO–Au NC, we obtain the effective distance between the donor and the acceptor, $r_{DA} \approx 2.55$ nm, using eqn (3) and (4). It is to be noted that the smaller value of r_{DA} compared to the radius of the ZnO NPs ($\sim$3 nm; Fig. 1a) can be rationalized from the fact that the origin of the PL peaking at 550 nm arises essentially from surface defects in the ZnO NPs.[32] Moreover, comparing the PL spectra of bare ZnO NPs and ZnO–Au NCs upon excitation above the band-edge, it was observed that the emission due to excitonic recombination is suppressed, while the defect-related emission is red shifted in the presence of Au NPs. In this respect, we have shown that the energy is transferred from the Vo^+ center to Au NPs which leads to a reduction in the PL intensity at 520 nm. The energy transfer efficiency (E) is found to be $\sim$19% (see ESI†, Fig. S4) which is a much lower value compared to that of below band-gap excitation ($E = \sim$85%). In retrospect, excited electrons are preferentially trapped by the V_O^{++} center, which is originated by V_O^+ by capturing a hole. The formation of V_O^{++} centers is more favorable upon band-edge excitation since the photogenerated holes have enough time to migrate during thermalization of highly excited electrons. This leads to more facile recombination of excited electrons *via* V_O^{++} centers, and this recombination pathway is supported by the appreciable red shift observed in ZnO–Au NCs upon above band-edge excitation. However, the decrease in band-edge emission intensity in the presence of Au NPs is well understood, whereby Au acts as

a sink which can store and shuttle photogenerated electrons.[16,33] As per our understanding, the optical activity of surface defect states in the overall emission of the semiconductor solely depends on the excitation wavelength.

3.2 Photoselective degradation of methylene blue

It was reported by several researchers that in the presence of metal NPs in close proximity to semiconductor NPs, enhanced photocatalytic degradation of test solutions was observed. Thus we compared the role of a Au layer in promoting photogenerated charges in ZnO–Au and ZnO colloids by carrying out photo-reduction of a test contaminant [MB, purchased from Carlo Erba]; MB is known to be an excellent probe for the study of interfacial electron transfer in colloidal semiconductor systems.[34] In general, the higher the charge migration from the surface of the ZnO semiconductor, the faster will be the degradation of the surface-attached MB. We have used a fiber-optic based system for the measurement of light-induced chemical processes with spectroscopic precision. To demonstrate the sensitivity and usefulness of our designed system, we previously conducted a detailed study of the photodeterioration of vitamin B2 (riboflavin) in aqueous phase.[35] In order to obtain different excitations we have used three different types of filters placed on a home-made UV bath (60 W; normally used for water purification). The optical filters, namely 420 high pass (HP), 460 low pass (LP) and 320 high pass (HP), were chosen in order to achieve controlled and preferential excitation. The characteristics of the optical filters are shown in Fig. 4a, which clearly depicts that 420 HP (passes light above 420 nm) is only used for the SP excitation of Au NPs, 460 LP (passes light below 460 nm) is used for the above band-edge excitation of ZnO, and the combined use of 320 HP and 460 LP (passes light above 320 nm and below 460 nm) leads to preferential excitation of below band-gap excitation of ZnO. In Fig. 4b, the relative concentration (C_t/C_0) of MB in solution is plotted with respect to UV irradiation time, the results of which indicate the photodegradation of MB upon continued UV irradiation. It is to be noted that there was no obvious
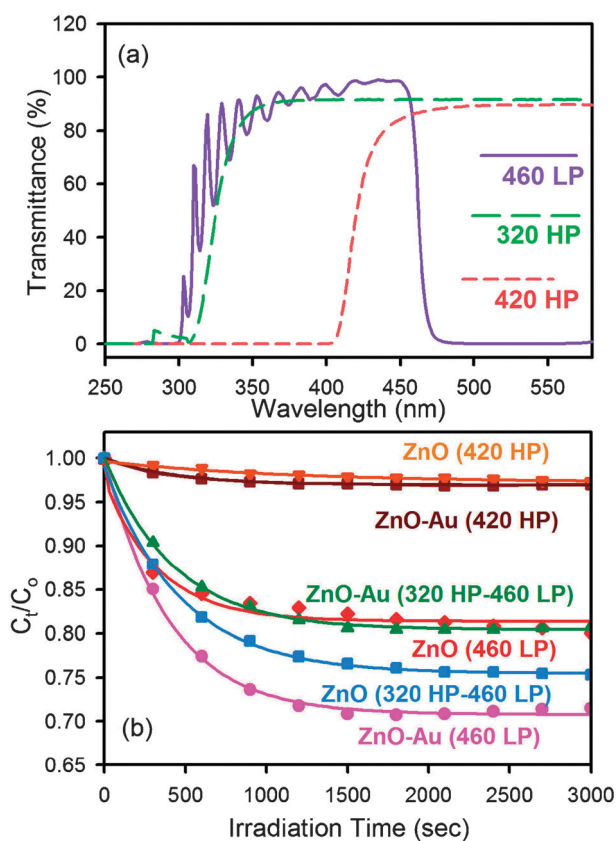
Fig. 4 (a) The transmittance spectra of 320 high pass (green), 420 high pass (red) and 460 low pass (violet) optical filters are shown. (b) Plot of relative concentration (C_t/C_0) *versus* time for the degradation of MB (monitored at 655 nm) is shown. The degradation is performed in the presence of colloidal solutions of ZnO NPs and ZnO–Au NCs under different excitation conditions (the optical filters used for the desired excitation are indicated in parentheses).

change in the concentration of MB stored in the dark for several hours (data are not shown here). Under selective UV radiation we have recorded the absorption peak of MB (at 655 nm) at 5 second intervals, using SPECTRA SUITE software supplied by Ocean Optics, and plotted it against the time of photo-irradiation. All the photodegradation curves were found to follow a first-order exponential equation, and the kinetic parameters are represented in Table 1. The decrease in the absorbance at 655 nm implies the generation of the colourless photoproduct Leuco-Methylene Blue (LMB). Note that in the present study we are interested in exploring the long-time photodegradation of MB (for several minutes). By comparing the photodegradation of MB in the presence of ZnO NPs and ZnO–Au NCs with a 420 HP filter, it is clearly shown that no considerable change in the absorbance peak at 655 nm takes place upon Au SP excitation. The photodegradation rates are found to be 1.055×10^{-3} s^{-1} and 1.388×10^{-3} s^{-1}, and the percentages of total photodegradation (*i.e.*, the value of A in the first-order kinetic equation shown in Table 1) are 2.66 and 2.78 for ZnO and ZnO–Au NCs, respectively. It reveals that electron transfer from Au NPs to MB is not allowed upon direct excitation of Au. Upon replacing the 420 HP filter with a 460 LP filter, we observed an increase in the photodegradation

rates in the presence of Au NPs ($k_{ZnO} = 2.203 \times 10^{-3}$ s^{-1}, $k_{ZnO-Au} = 2.258 \times 10^{-3}$ s^{-1}), and the percentage of photodegradation also improved from $A_{ZnO} = 11.68$ to $A_{ZnO-Au} = 29.31$. This is attributed to improved charge separation in the presence of Au NPs which also can store and shuttle excited electrons, thereby suppressing recombination. Such Au NP-stabilized ZnO NPs behave as more efficient electron accumulators (at the conduction band) than the bare oxide.[36] In retrospect, the photodegradation rate of MB was observed to decrease ($k_{ZnO} = 2.340 \times 10^{-3}$, $k_{ZnO-Au} = 2.287 \times 10^{-3}$), and the percentage of total photodegradation was found to be much lower ($A_{ZnO} = 23.55$, $A_{ZnO-Au} = 19.65$) in the presence of Au NPs when we used combined optical filters of 320 HP and 460 LP. This happens because excited electrons of ZnO can easily occupy the defect centers and resonantly transfer their energy to Au NPs *via* non-radiative processes (FRET, as previously discussed). As a consequence, in the presence of Au, excited electrons are unable to migrate from the ZnO surface to perform the reduction of MB. Thus, it is important to note that the differences in rate constants are not significant, whereas considerable differences in the magnitude of total photodegradation are observed during above band-edge and below band-gap excitation of ZnO and ZnO–Au NCs. This is due to the fact that the total number of active electrons available for carrying out MB degradation is different for ZnO and ZnO–Au NCs for any particular excitation. Our study clearly demonstrates that the role of an incorporated metal on a semiconductor for facilitating redox reactions is solely dependent on the excitation of the semiconductor.

3.3 Optimized dye-sensitized solar cell performance

The efficient charge migration in metal–semiconductor NCs is expected to lead to improved DSSC performance of ZnO–Au NCs compared to bare ZnO. Thus, we measured and directly compared the incident photon-to-current conversion efficiency (IPCE) of ZnO and ZnO–Au based DSSCs. The IPCE, defined as the number of electrons collected per incident photon, was evaluated from short-circuit photocurrent (J_{sc}) measurements at different wavelengths (λ), and the IPCE was calculated using eqn (5),

$$IPCE\% = [1240 \times J_{SC}(A\ cm^{-2})]/[\lambda(nm) \times P(W\ cm^{-2})] \times 100\% \qquad (5)$$

where P is the incident light power. Each of the two examined ZnO and ZnO–Au based cells contained the same sensitizer dye N719 and I^-/I_3^- electrolyte, to allow for a fair comparison. The IPCE curves of the two cells are presented in Fig. 5a which shows a broad spectral response in the range 440 to 600 nm. Significant enhancement in photocurrent generation is seen upon deposition of Au NPs on the ZnO electrodes. The enhancement in the photocurrent generation efficiency is indicative of the fact that the Au NPs assist in the charge separation within the nanostructured ZnO film as well as improve the interfacial charge transfer processes.

Fig. 5b shows the photocurrent–voltage ($J–V$) characteristics for solar cells, constructed using the bare ZnO NPs and ZnO–Au NCs. The short-circuit current density (J_{sc}) and the

This journal is © the Owner Societies 2011

Phys. Chem. Chem. Phys., 2011, **13**, 12488–12496 | 12493
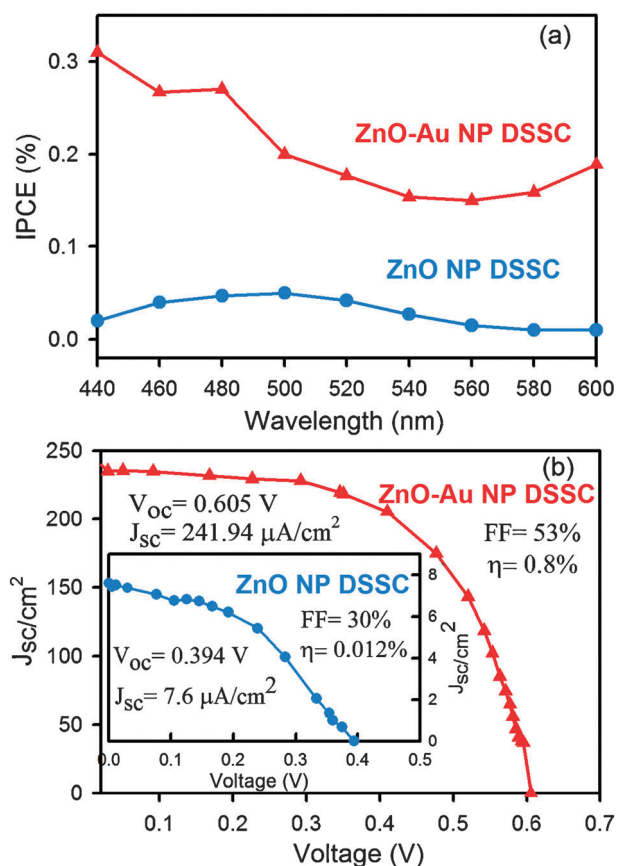
Fig. 5 (a) Dependence of the incident photon conversion efficiency on the incident wavelength for ZnO NP (blue) and ZnO–Au NC (red) films cast on an FTO plate. (b) Photocurrent–voltage (J–V) characteristics of ZnO–Au NC and ZnO NP (inset) based DSSC (with 10.5 klux illumination intensity at the area of 0.16 cm^2 from a 90 W xenon lamp).

open circuit voltage (V_{oc}) of the ZnO–Au NC-based DSSC were 261.87 µA cm^{-2} and 0.605 V, respectively, which are much higher than that of the bare ZnO based DSSC (J_{sc} = 7.5 µA cm^{-2}, V_{oc} = 0.394 V). The fill factor (FF) and power conversion efficiency (η) of the solar cells can be determined from eqn (6) and (7),

$$FF = V_M J_M / V_{OC} J_{SC} \qquad (6)$$

$$\eta = V_{OC} J_{SC} / FF \qquad (7)$$

where V_M and J_M are the voltage and current density at the maximum power output, respectively.[37,38] The calculated values of FF and the overall power conversion efficiency of the ZnO-based DSSC were 30% and 0.012%, respectively, which are substantially improved in the presence of gold

Table 2 Device performance[a] of the dye-sensitized solar cells with ZnO NP and ZnO–Au NC

Device with N719	V_{OC}/V	J_{SC}/µA cm^{-2}	FF (%)	η (%)
ZnO NP	0.394	7.5	44	0.012
ZnO–Au NC	0.605	261.87	53	0.8

[a] Short-circuit photocurrent densities (J_{sc} cm^{-2}), open-circuit voltage (V_{oc}), fill factor (FF), and efficiency (η).

(FF = 53% and η = 0.8%). Table 2 summarizes the measured and calculated values obtained from each J–V curve.

The photoconductivity measurement[39,40] of the ZnO NP and ZnO–Au NC thin films was necessary in order to further understand the electron mobility (i.e. performance of the semiconductor) and charge transfer mechanism. At a fixed bias voltage of 5 V, the photocurrent across the thickness of the thin films was measured by using FTO as one of the electrodes and a small (4 mm diameter) drop of mercury (Hg) on top of the film as a counter electrode. The light source (intensity 25 mW cm^{-2}) was turned ON and OFF every 20 seconds, and the obtained current values were continuously recorded using a programmable multimeter (Gwinstek GDM-396). Fig. 6 shows the photocurrent response for the ZnO NP and ZnO–Au NC thin films, where an improved photocurrent was observed for the ZnO–Au NC thin film ($\sim$70 µA) under illuminated condition compared to the ZnO NP thin film ($\sim$1.5 µA). This shows that the photogenerated electrons in ZnO NPs (from visible light absorption by the intermediate Vo^+ center) are transferred to Au NPs, as mentioned earlier contributing in enhanced photocurrent of the ZnO–Au NC thin films compared to the ZnO NP. In the case of the model DSSC shown here, a similar mechanism is responsible for the enhanced photocurrent observed (Fig. 5b) in the presence of Au NPs along with the ZnO NPs. Some of the injected electrons from the excited N719 dye to the CB of ZnO are captured by the intermediate defect sites of ZnO (Vo^+) resulting in poor photocurrent and fill factor of DSSC. However, in the presence of Au NPs in the ZnO thin film, we have observed higher photocurrent (J_{sc} = 261.87 µA cm^{-2}) and fill factor (FF = 53%) compared to the ZnO NP DSSC (J_{sc} = 7.5 µA cm^{-2} and FF = 44%). Thus, it is noted that the ratios of improved photocurrent response (70 : 1.5) and short-circuit current (261.87 : 7.5) for ZnO and ZnO–Au semiconductors are comparable. The improvement observed in the overall device performance is mainly due to increased conductivity by transferring the trapped electrons in Vo^+ centers of ZnO to Au NPs which then contribute to the photocurrent as well as the fill factor of the DSSC. It is worth noting that the efficiency obtained from the model DSSC with
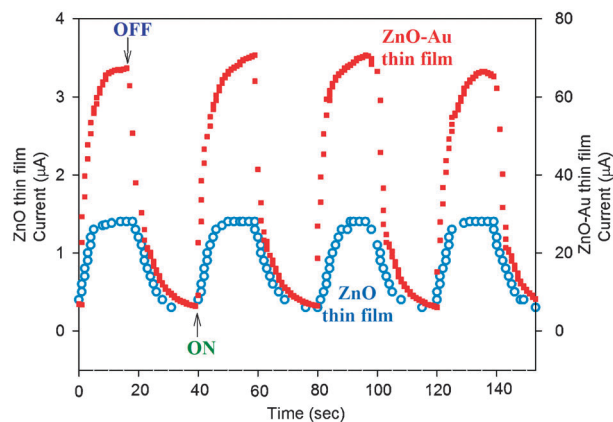

Fig. 6 Photocurrent responses of ZnO NP and ZnO–Au NC thin films under bias voltage of 5 V. The photocurrent was measured across the thickness of the films with 25 mW cm^{-2} incident power from a halogen light source.

the use of NPs is lower than the maximum efficiency reported[41] with nanorods, which were employed to provide higher surface area and better charge transport.

4. Conclusions

In conclusion, the present study provides a mechanistic explanation for the excitation-dependent recombination processes and the catalytic activity of Au NPs in the ZnO–Au NCs, as schematically shown in Scheme 1. A better understanding of the charge-transfer processes at the semiconductor/metal interface is crucial for optimizing the performance of such catalysts. Our results demonstrate that the excited ZnO NPs resonantly transfer visible optical radiation to the Au NPs upon below band-gap excitation of the semiconductor. A singly charged vacancy center of the ZnO semiconductor is demonstrated to be responsible for the visible optical radiation transfer from ZnO NPs to Au NPs, whereas, a combination of the energy transfer between surface defects and SP of Au NPs, as well as thermalization of photogenerated electron–hole pairs and their recombination in the ZnO NPs is believed to take place simultaneously upon above band-edge excitation. We observe that the prepared ZnO–Au NCs are stable and efficient enough for the environmental purification of organic pollutants. As a low cost photovoltaic cell, the incident photon-to-current conversion efficiency and short-circuit current are significantly improved in the presence of Au NPs which is attributed to the better electron mobility of the ZnO–Au semiconductor. This approach may give rise to a new class of multifunctional materials with possible applications in energy-conversion devices and biofunctionalized materials.
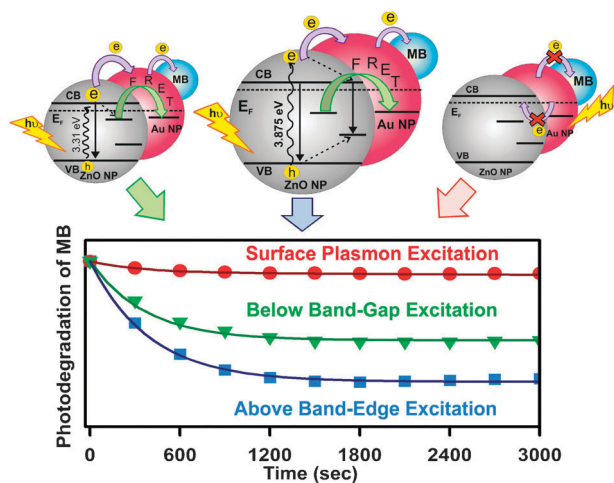
Scheme 1 Schematic representation of the metal–semiconductor system: the system consists of a semiconductor ZnO NP (gray big ball) containing appreciable amounts of defect states on which a Au NP (red big ball) is fabricated. Methylene Blue (small blue ball) is bound to the ZnO–Au NC by surface adsorption. The dynamics of charge separation and interparticle charge/energy migration of the entire structure is shown. Thereafter, photodegradation of Methylene Blue under different excitation conditions is also shown by a graph which reveals the mediating role of Au NP in photocatalysis.

Notes and references

1 C. B. Murray, C. R. Kagan and M. G. Bawendi, *Science*, 1995, **270**, 1335–1338.
2 A. Henglein, *Chem. Rev.*, 1989, **89**, 1861–1873.
3 T. Y. Olson and J. Z. Zhang, *J. Mater. Sci. Technol.*, 2008, **24**, 433–446.
4 M. A. Sliem, T. Hikov, Z. A. Li, M. Spasova, M. Farle, D. A. Schmidt, M. H. Newen and R. A. Fischer, *Phys. Chem. Chem. Phys.*, 2010, **12**, 9858–9866.
5 X. S. Fang, T. Y. Zhai, U. K. Gautam, L. Li, L. M. Wu, Y. Bando and D. Golberg, *Prog. Mater. Sci.*, 2011, **56**, 175–287.
6 S. Link and M. A. El-Sayed, *J. Phys. Chem. B*, 1999, **103**, 8410–8426.
7 R. Jin, Y. C. Cao, C. A. Mirkin, K. L. Kelly, G. C. Schatzand and J. G. Zheng, *Science*, 2001, **294**, 1901–1903.
8 P. V. Kamat, *J. Phys. Chem. B*, 2002, **106**, 7729–7744.
9 M. Valden, X. Lai and D. W. Goodman, *Science*, 1998, **281**, 1647–1650.
10 M. Haruta, *Catal. Today*, 1997, **36**, 153–166.
11 Z. H. Chen, Y. B. Tang, C. P. Liu, Y. H. Leung, G. D. Yuan, L. M. Chen, Y. Q. Wang, I. Bello, J. A. Zapien, W. J. Zhang, C. S. Lee and S. T. Lee, *J. Phys. Chem. C*, 2009, **113**, 13433–13437.
12 Y. Tian and T. Tatsuma, *J. Am. Chem. Soc.*, 2005, **127**, 7632–7637.
13 V. Subramanian, E. E. Wolf and P. V. Kamat, *J. Phys. Chem. B*, 2001, **105**, 11439–11446.
14 N. Chandrasekharan and P. V. Kamat, *J. Phys. Chem. B*, 2000, **104**, 10851–10857.
15 A. Wood, M. Giersig and P. Mulvaney, *J. Phys. Chem. B*, 2001, **105**, 8810–8815.
16 V. Subramanian, E. E. Wolf and P. V. Kamat, *J. Phys. Chem. B*, 2003, **107**, 7479–7485.
17 M. Jakob and H. Levanon, *Nano Lett.*, 2003, **3**, 353–358.
18 C. C. Li, L. M. Li, Z. H. Du, H. C. Yu, Y. Y. Xiang, Y. Li, Y. Cai and T. H. Wang, *Nanotechnology*, 2008, **19**, 035501.
19 K. Shibahara, N. Kuroda, S. Nishino and H. Matsunami, *Jpn. J. Appl. Phys.*, 1987, **26**, 1815–1817.
20 Y. W. Heo, D. P. Norton and S. J. Pearton, *J. Appl. Phys.*, 2005, **98**, 073502.
21 C. C. Lin, H. P. Chen, H. C. Liao and S. Y. Chen, *Appl. Phys. Lett.*, 2005, **86**, 183103–183105.
22 N. Ohashi, T. Ishigaki, N. Okada, T. Sekiguchi, I. Sakaguchi and H. Haneda, *Appl. Phys. Lett.*, 2002, **80**, 2869.
23 J. M. Lin, H. Y. Lin, C. L. Cheng and Y. F. Chen, *Nanotechnology*, 2006, **17**, 4391–4394.
24 C. W. Cheng, E. J. Sie, B. Liu, C. H. A. Huan, T. C. Sum, H. D. Sun and H. J. Fan, *Appl. Phys. Lett.*, 2010, **96**, 071107.
25 J. R. Lakowicz, *Principles of Fluorescence Spectroscopy*, Kluwer Academic/Plenum Publishers, New York, 2nd edn, 1999.
26 M. Haase, H. Weller and A. Henglein, *J. Phys. Chem.*, 1988, **92**, 482–487.
27 A. van Dijken, E. A. Meulenkamp, D. Vanmaekelbergh and A. Meijerink, *J. Phys. Chem. B*, 2000, **104**, 1715–1723.
28 K. Vanheusden, W. L. Warren, C. H. Seager, D. R. Tallant and J. A. Voigt, *J. Appl. Phys.*, 1996, **79**, 7983.

This journal is © the Owner Societies 2011

Phys. Chem. Chem. Phys., 2011, **13**, 12488–12496 | 12495

29 J. D. Ye, S. L. Gu, F. Qin, S. M. Zhu, S. M. Liu, X. Zhou, W. Liu, L. Q. Hu, R. Zhang, Y. Shi and Y. D. Zheng, *Appl. Phys. A: Mater. Sci. Process.*, 2005, **81**, 759–762.

30 M. Ghosh and A. K. Raychaudhuri, *Nanotechnology*, 2008, **19**, 445704.

31 H. M. Watrob, C. P. Pan and M. D. Barkley, *J. Am. Chem. Soc.*, 2003, **125**, 7336–7343.

32 A. Makhal, S. Sarkar, T. Bora, S. Baruah, J. Dutta, A. K. Raychaudhuri and S. K. Pal, *Nanotechnology*, 2010, **21**, 265703.

33 V. Subramanian, E. E. Wolf and P. V. Kamat, *J. Am. Chem. Soc.*, 2004, **126**, 4943–4950.

34 S. Baruah, S. S. Sinha, B. Ghosh, S. K. Pal, A. K. Raychaudhuri and J. Dutta, *J. Appl. Phys.*, 2009, **105**, 074308.

35 S. S. Sinha, P. K. Verma, A. Makhal and S. K. Pal, *Rev. Sci. Instrum.*, 2009, **80**, 053109.

36 P. D. Cozzoli, M. L. Curri and A. Agostiano, *Chem. Commun.*, 2005, 3186–3188.

37 Y. B. Tang, Z. H. Chen, H. S. Song, C. S. Lee, H. T. Cong, H. M. Cheng, W. J. Zhang, I. Bello and S. T. Lee, *Nano Lett.*, 2008, **8**, 4191–4195.

38 W. J. E. Beek, M. M. Wienk and R. A. J. Janssen, *Adv. Funct. Mater.*, 2006, **16**, 1112–1116.

39 L. Hu, J. Yan, M. Liao, L. Wu and X. Fang, *Small*, 2011, **7**, 1012–1017.

40 X. Fang, Y. Bando, M. Liao, U. K. Gautam, C. Zhi, B. Dierre, B. Liu, T. Zhai, T. Sekiguchi, Y. Koide and D. Golberg, *Adv. Mater.*, 2009, **21**, 2034–2039.

41 K. Keis, E. Magnusson, H. Lindstrom, S. E. Lindquist and A. Hagfeldt, *Sol. Energy Mater. Sol. Cells*, 2002, **73**, 51–58.